Chapter 5

Simulating Galaxy-Galaxy Interactions

5.1 Introduction

Mergers and other gravitational interactions between galaxies are an essential part of hierarchical galaxy formation scenarios (White and Rees (1978)). Mergers can have a dramatic effect on the structure of galaxies. It was first noted by Toomre (1977) that galaxy collisions can drive the evolution of galaxy types by transforming disk galaxies into elliptical galaxies. Additionally galaxy mergers are thought to explain the extremely high levels of star formation seen in high redshift ultra-luminous infrared galaxies (e.g. Sanders et al. (1988))

In this chapter we present simulations of interacting disk galaxies. In section 5.2 we discuss the initial conditions of the simulations. In section 5.3 we introduce the specific simulations that were run and in sections 5.4 and 5.5 we analyse the interacting galaxies in terms of the structure of the tidal tails, and the properties and structure of the resulting remnant. Additionally these simulations provide an ideal way of testing the performance of the sticky particle star formation and feedback model in a more dynamic situation than the isolated galaxies discussed in previous chapters.

We conclude this chapter by simulating the formation of a disk galaxy in a fully cosmological setting.

5.2 Initial Conditions

The most favourable conditions for the creation of tidal tails are interactions in which the angular momentum vectors of the individual galactic disks (spin angular momentum)
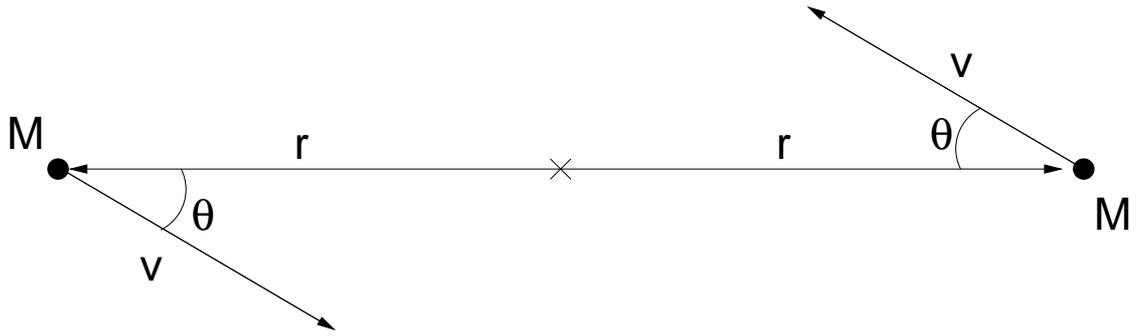
Figure 5.1: Geometry used in the galaxy collision simulations. The circles represent the initial locations of the galaxies. They are separated by an amount $2r$, moving with a velocity v and each has mass M.

are aligned with the angular momentum vector of the orbit (orbital angular momentum) of the galaxies around each other (Springel and White (1999)). Since here we are trying to form prominent tidal tails we usually set up the disk-disk collisions on these types of orbits. The properties of the individual disks are as described in section 4.2.1. The geometry of the initial conditions is described in figure 5.1. We need to specify five numbers to completely define a set of initial conditions: $2r$, the separation between the two disks; 2θ the angle between their velocity vectors; $|v|$, the magnitude of the relative velocities; ψ, the angle between the spin vectors of the two galaxies and M, the mass of each galaxy.

The initial separation of the disks is always set to twice the virial radius of their respective dark matter haloes ($r = r_v$). The magnitude of the velocity is set such that the interaction is 'parabolic' (the total energy of the system is 0). θ is set by considering the 'circularity' of the interaction, which is defined as (Lacey and Cole (1993))

$$\epsilon = \frac{J}{J_c(E)} \, ,$$
(5.1)

where J is the orbital angular momentum of the galaxies and $J_c(E)$ is the orbital angular momentum of a circular orbit with the same energy, E. Radial orbits have $\epsilon = 0$ and circular orbits have $\epsilon = 1$. Typical galaxy-galaxy interactions have a circularity of ~ 0.5 (Tormen (1997)). For the collision geometry described above, the circularity of the orbit is given by

$$\epsilon = \sin \theta \, .$$
(5.2)

5.3 Simulations

The galaxy collision simulations we ran fall into two main groups; those that are designed to allow us to probe the properties of tidal tails and those that are designed to form an elliptical galaxy to allow us to investigate the properties of the resulting remnant. In all simulations the two galaxies start off separated by 200 kpc, simulations were run with circularities of 0.0,0.2 and 0.5. Initial conditions were set up as described in the previous section.

An additional simulation was run with initial conditions that approximate the interaction between the MW and M31. In this case, properties of the initial conditions are set via observation as possible. The ratio of the galaxy masses is somewhat uncertain and has been estimated as 1:0.7 (Dunn and Laflamme (1993)), 1:0.625 (Klypin et al. (2002)) and 1.25:1 (Seigar et al. (2006)). Due to this uncertainty we assume in our simulations that the galaxies are of equal mass. The initial separation between the galaxies is 780kpc (Holland (1998)) and their initial relative radial velocity is 123 km/s (Dunn and Laflamme (1993)). The galactic latitude of M31 is -21.57 degrees[1], and its disk is tilted at an angle of 77.5 degrees to our line of sight (Schmidt (1957); Ma et al. (1997)). The tangential velocity of the Andromeda galaxy relative to the MW is hard to constrain via observation. It has long been suspected that this tangential velocity must be small, given that there is no other large galaxy in the local group to impart much angular momentum to the M31-Milky Way system (Kahn and Woltjer (1959)). Under the assumption that the Milky Way and M31 have equal but opposite angular momenta Einasto and Lynden-Bell (1982) estimated that the tangential velocity of M31 is 60 ± 30km/s. This is in agreement with studies using the 'least action principle' (Peebles (1989, 1990)). The least action principle assumes that each galaxy can be treated as a point particle and then setting two boundary conditions. Firstly at early times the peculiar velocities of all galaxies are small and secondly that at late times the position of each galaxy is known. It is possible to numerically iterate over trial orbits until we find the one that minimises the 'action' of the system. Recent least action principle studies of the local group suggest that the transverse velocity of M31 is less than 100km/s (Peebles et al. (2001)). We therefore use a value of 60km/s for the transverse velocity of M31.

---

[1]via NED

5.4   Star Formation in Tidal Tails

Tidal tails are produced during galaxy collisions from the effects of gravitational tides and galactic rotation (Toomre and Toomre (1972)). Tails may be ejected over 100kpc from the merger remnant, and some fraction may become completely unbound from the rest of the system. Evidence for strong star formation in tidal arms comes from the fact that they are often blue (Schombert et al. (1990)), in some tidal features it is possible to detect $H\alpha$ and UV (Neff et al. (2005)) emission, also indicative of strong star formation. The inferred ages of stars forming in tidal arms is much less than the dynamical timescales on which the tidal arms are evolving and so it may be assumed that the stars are forming in the tidal arms themselves (Knierman et al. (2003)). It has been predicted (Barnes and Hernquist (1992); Mihos and Hernquist (1994a)) that the collapse of gas in tidal arms could lead to the formation of 'tidal dwarf galaxies', this has been borne out by observations of star forming clumps in the tidal arms of various interacting galaxies, which are found to have masses in the range $10^{8.3} - 10^{9.8} M_\odot$ (Duc and Mirabel (1998)), consistent with the masses of observed dwarf galaxies.

Figures 5.2 and 5.3 show the locations of particles in the stellar disk of the galaxy and the resulting projected temperature structure of the Milky Way/M31 interacting galaxy simulation. The formation of strong tidal features is evident. Gas within the tidal arms cools to $\sim 10^4$K, HII regions due to gas heating by supernovae are also evident. At late times the merger remnant contains very little cold gas, in common with elliptical galaxies observed in the local universe (see next section).

It is hard to objectively quantify either the mass or the extent of tidal arms during an interaction. We follow Springel and White (1999) by using the tidal response, T, defined here as the fraction of the mass of a disk that reaches a distance of more than $3R_D$ from its centre of mass, where R_d is the unperturbed initial truncation radius of the disk. Figure 5.5 shows the evolution of the tidal response of three galaxy interaction simulations as a function of time. There is a clear correlation between the height of the peak in the tidal response and the initial circularity of the orbit, in agreement with the results of Springel and White (1999), suggesting that in order to probe the properties of tidal tails we should be colliding galaxies on nearly circular orbits.

Since stars form from molecular gas, an understanding of the physical properties and kinematics of the molecular phase in tidal arms is very important in the study of the formation of tidal dwarf galaxies. Figure 5.6 shows contours of molecular gas density

on top of a greyscale representation of the atomic gas density in an interacting galaxy pair. The contours of molecular gas density are chosen to match those used by Wilson et al. (2000) in their high-resolution images of molecular gas in the antennae galaxies. In common with Wilson et al. (2000) we find strong peaks in the molecular gas density coincident with the nuclei of each galaxy. Molecular gas is also present in the tidal features around the galaxy and in the region between the two nuclei, which in the case of the antennae galaxies has been named the 'overlap region' Stanford et al. (1990). It has long been known (van der Hulst (1979) that the majority ($> 60\%$) of the molecular gas in typical mergers is found in the tidal arm structures. Our simulations reproduce this, with 62% of the molecular gas being situated further than $3R_d$ from the centre of mass of either of the disks.

In this section we have investigated some of the basic properties of tidal arms and found that our statistical model reproduces very well many of their observed features. It remains as future work (see chapter 6) to apply our model to simulations designed to match the properties of real galaxy mergers.

5.5   Merger Remnants

In this section we compare the properties of the merger remnants left over from the merger of two equal mass disks, the initial configuration of this simulation is as described in the MW/M31 interaction. Results are compared both to other simulations and, where possible, to observational data from local elliptical galaxies.

The total amount of molecular gas in the remnant is $\sim 10^8 M_\odot$, this is in good agreement with observational studies of local early type galaxies (see e.g. Faber et al. (1997))

Previous galaxy merger simulations by Barnes (1992) have concentrated on the kinematics and orbital structure of the resulting galaxy. We find in common with these simulations that the radial density profile of the stellar material in the remnant is well fit by a broken power law with indices -2 toward the interior of the galaxy and -4 towards the outskirts (figure 5.7). The projected brightness profile of the galaxy is well described by the standard de Vaucouleurs law

$$\Sigma(r) = \Sigma_0 e^{[-(r/r_e)^{0.25} - 1]} , \qquad (5.3)$$

where $\Sigma(r)$ is a surface brightness and the two parameters that control the fit are Σ_0, the central brightness and r_e the effective radius of the galaxy. Magnitudes were calcu-
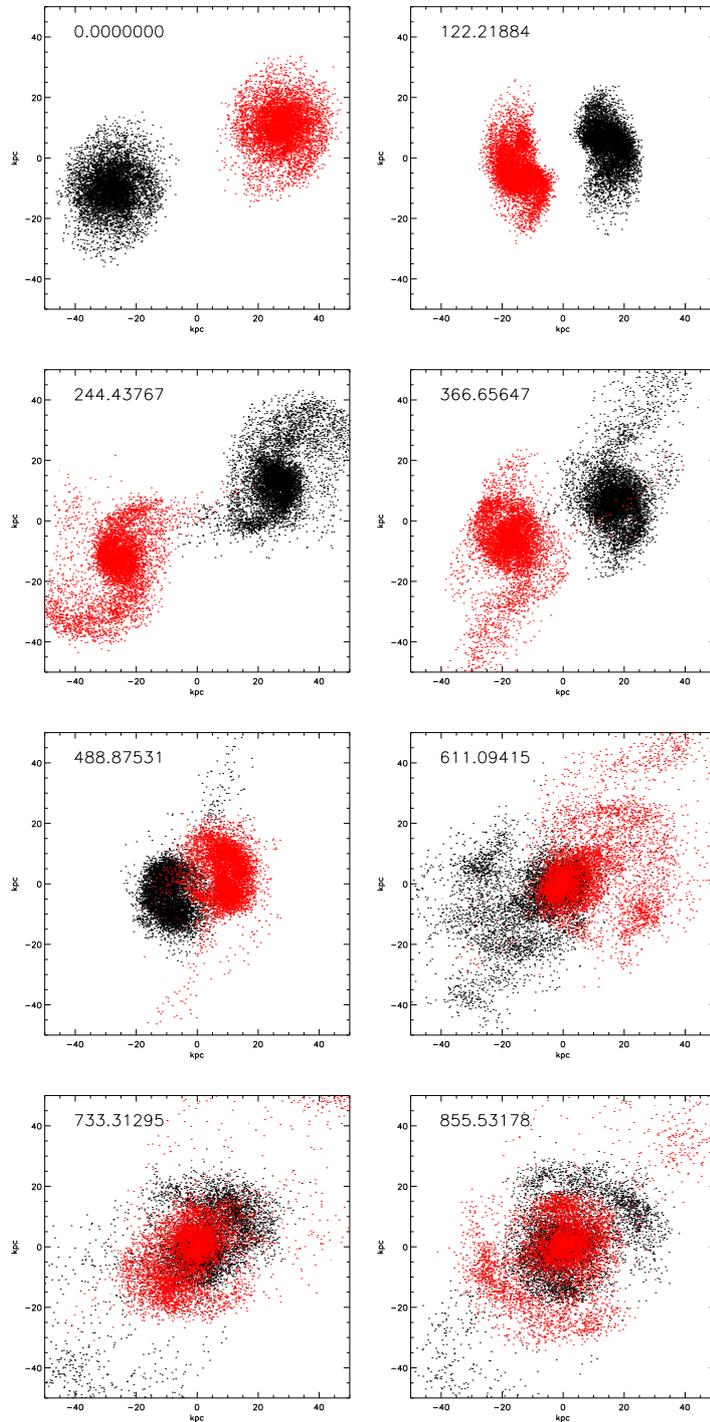
Figure 5.2: Time series showing the location of a random 10% of the particles in the old stellar disk of the galaxies. The numbers represent times in units of Myr
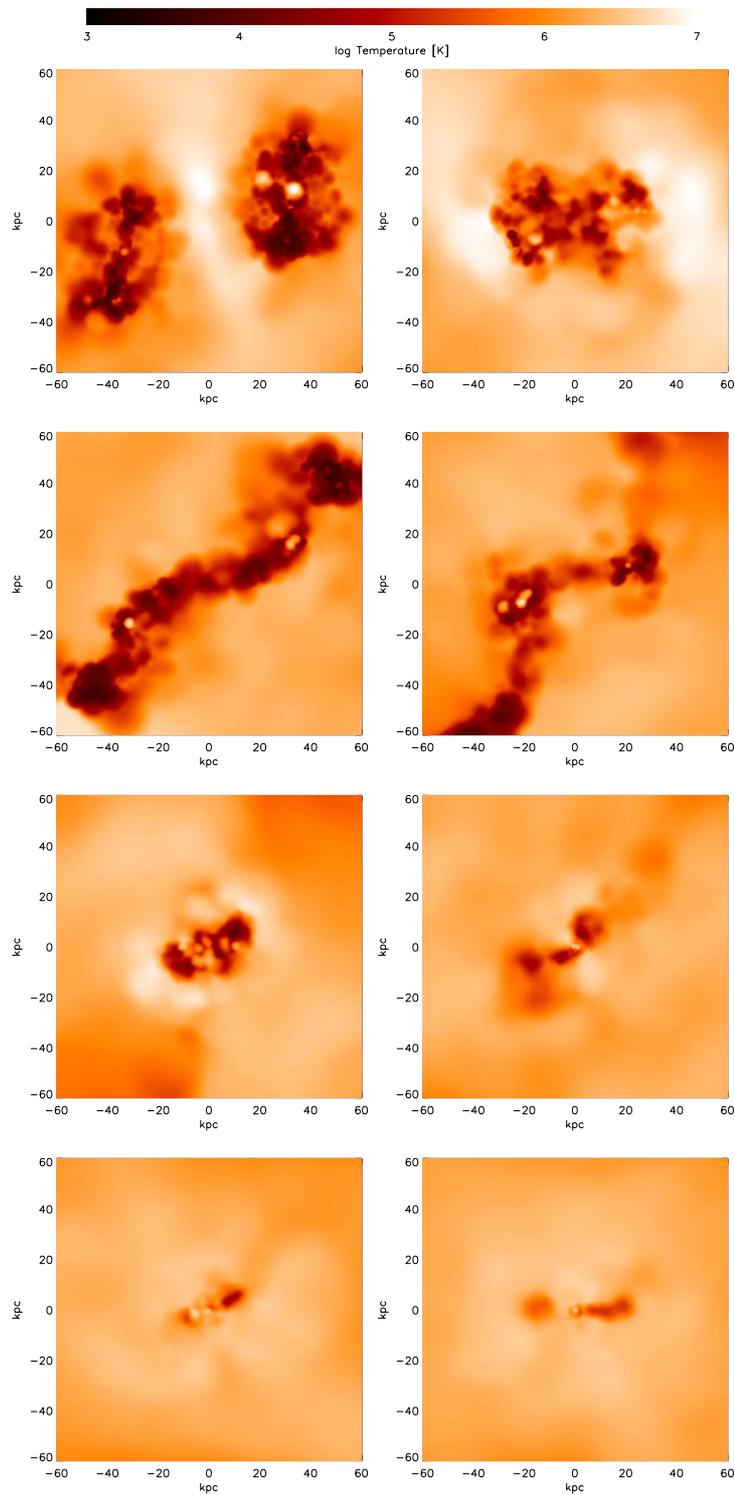
Figure 5.3: Projected mean temperature maps through the merging galaxy. Gas associated with the galaxy is dense enough to allow it to cool to temperatures of $\sim 10^4$K. The times of these snapshots match with those in the previous figure
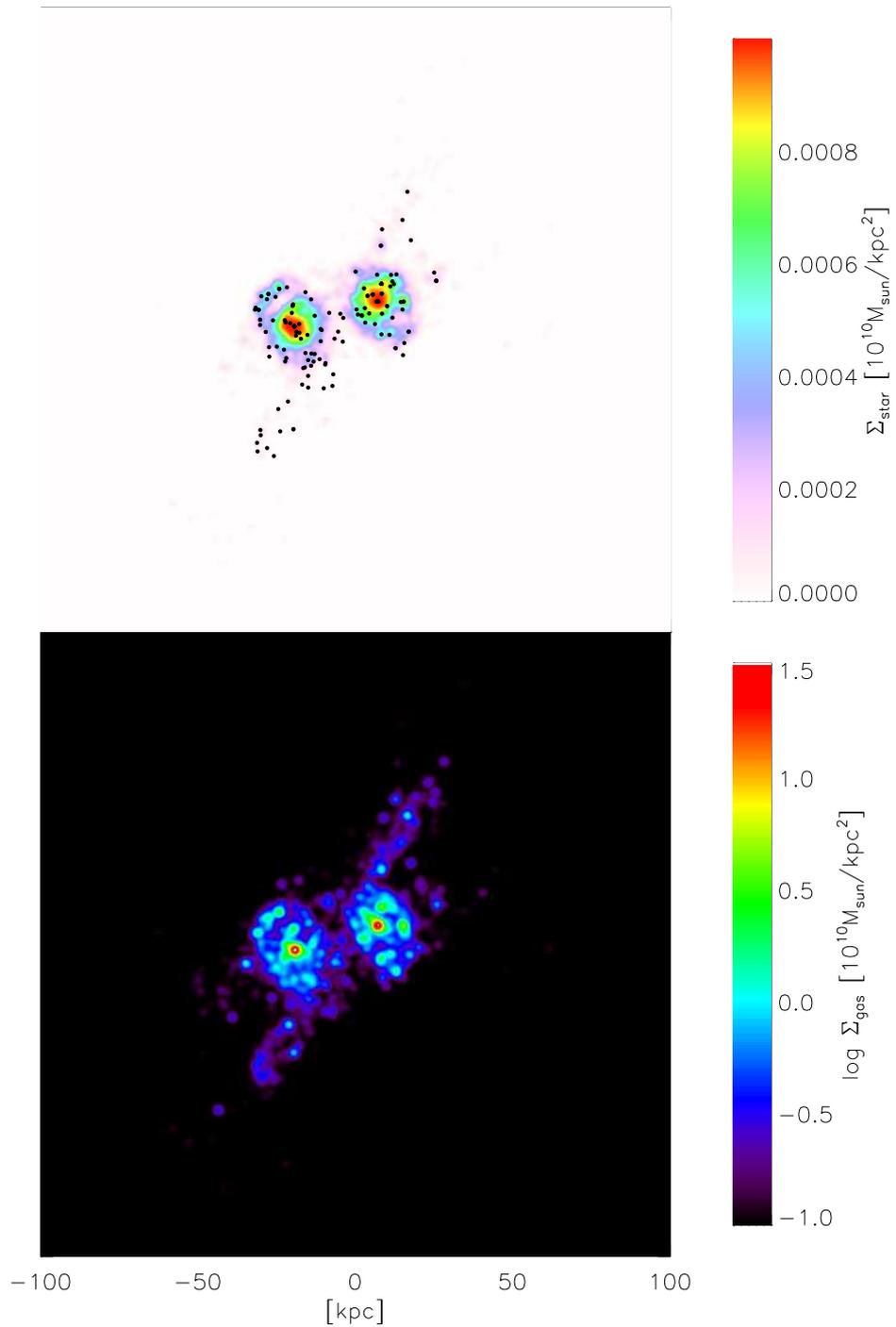
Figure 5.4: Snapshot of interacting galaxies. The upper panel shows contours of stellar density, including all stars. The black points represent sites of star formation within the last 10Myr. It is clear that star formation is occurring in the tidal arms of the galaxy. The lower plot shows the density of gas in the simulation.
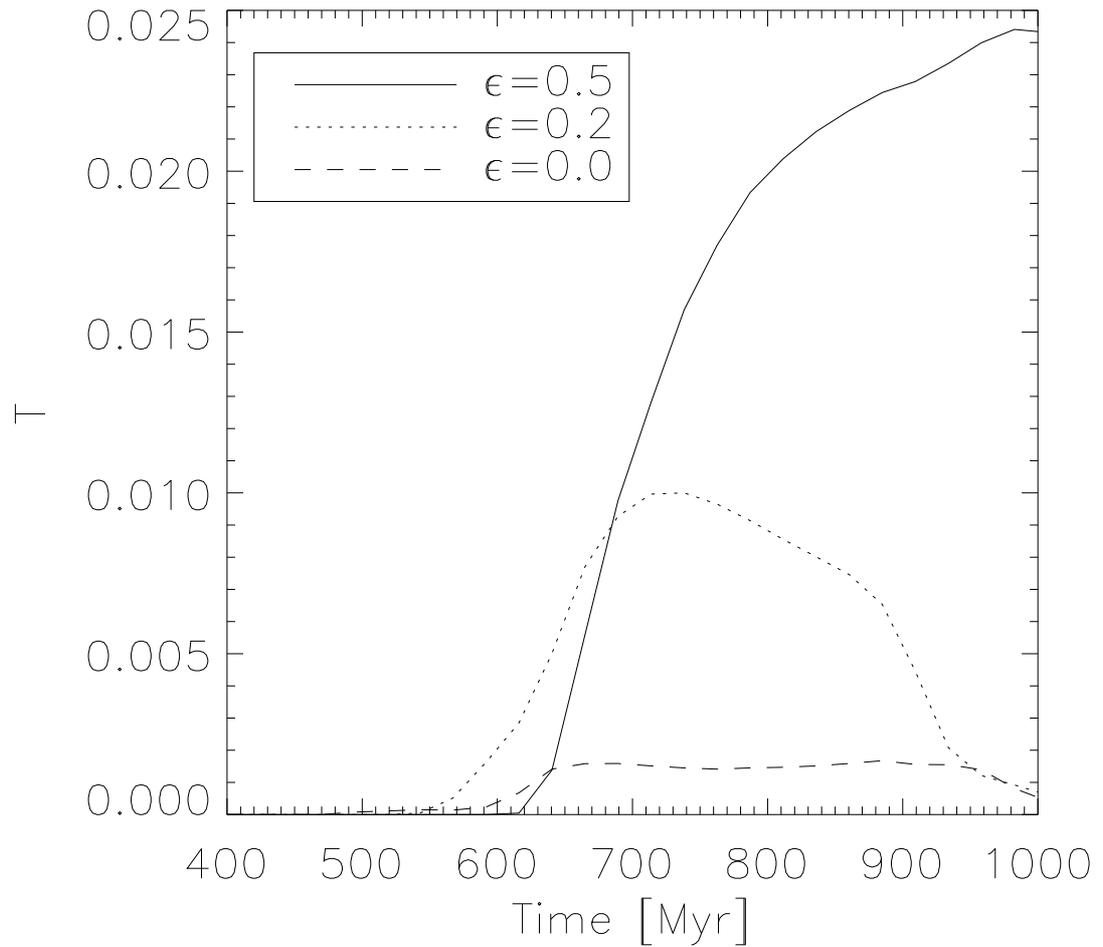
Figure 5.5: The tidal response of the three galaxy collision simulations. The tidal response is defined at the fraction of the mass of a disk that moves to a distance $> 3R_d$ from its centre of mass. There is a clear correlation between the tidal response of a collision and the circularity of the initial orbits.
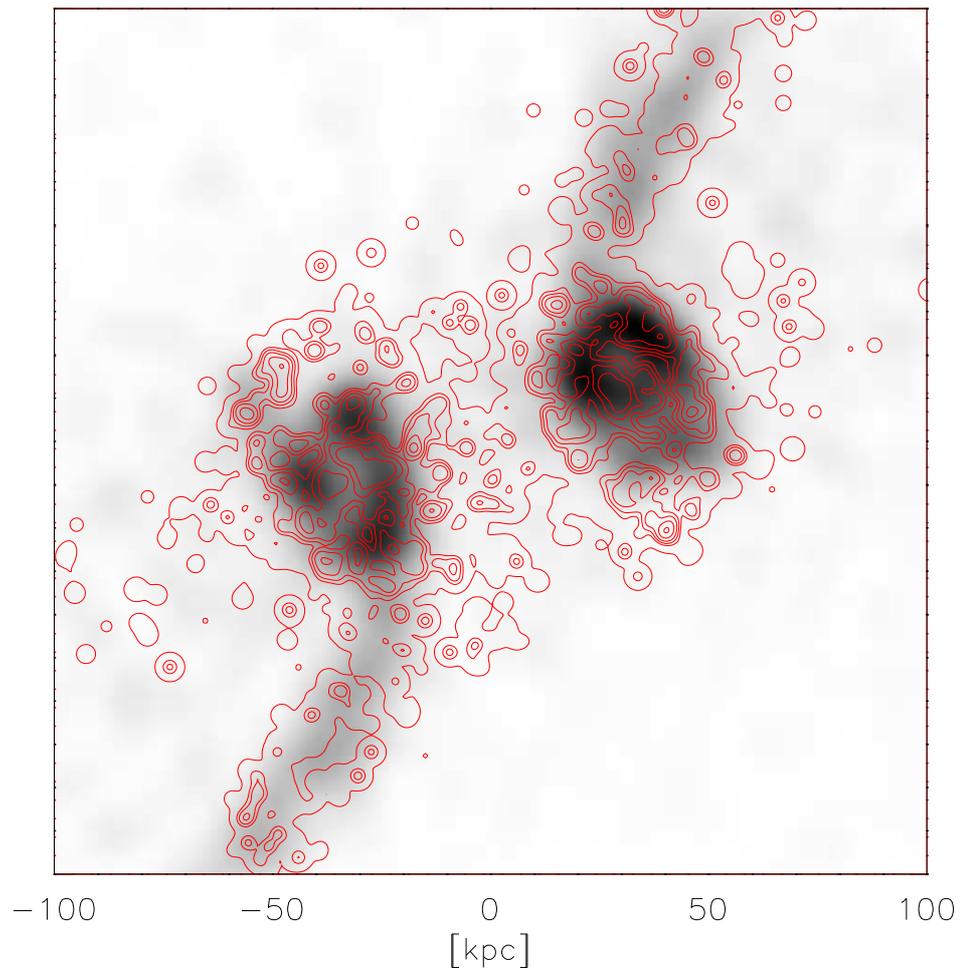
Figure 5.6: The distribution of molecular gas in the interacting galaxy pair. The greyscale image represents the density of atomic hydrogen in the galaxy. The contours show the density of molecular gas. Contours are chosen to match the plots of Wilson et al (2000) and represent 6%, 9.5%, 15%, 23%, 37% and 57% of the peak intensity.
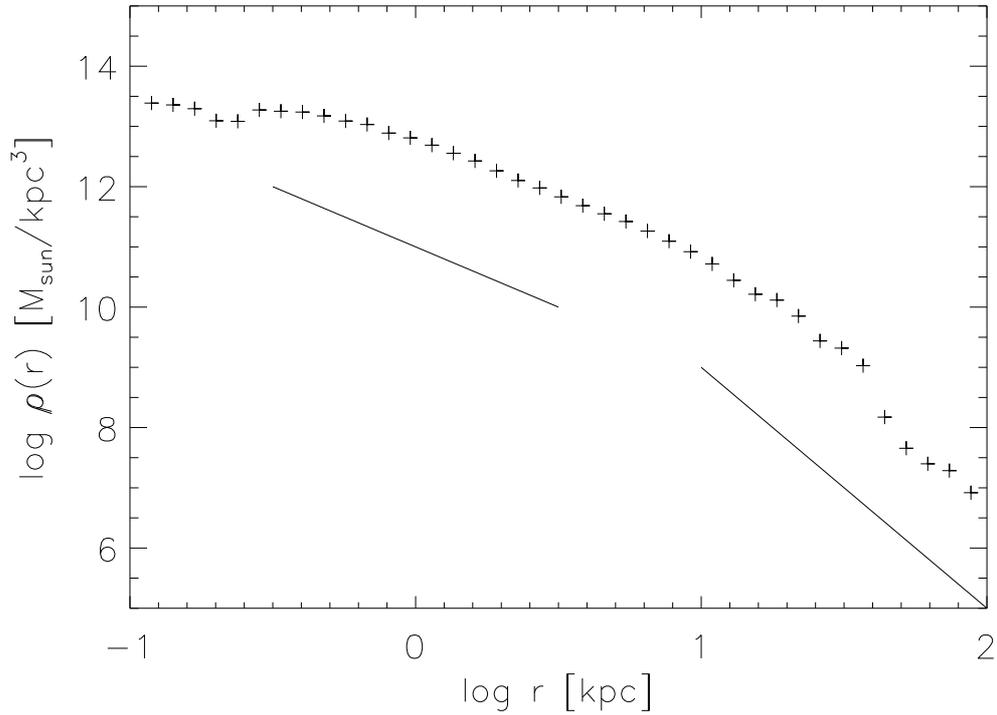
Figure 5.7: The radial stellar density profile of the merger remnant. The diagonal lines are power laws with indices -2 and -4, as observed in the simulations of Barnes (1992)

lated crudely from stellar masses by assuming that the flux from any given particle is proportional to its mass, then calculating the magnitude from $m = -2.5 \log(flux)$. This approximation is very crude and it remains as future work (see chapter 6) to include stellar population synthesis models (e.g. Bruzual and Charlot (1993)) in our code in order to provide more accurate observational constraints on the stellar features of our galaxy.

X-ray studies of local early-type galaxies have found evidence for hot gas haloes (see e.g. Forman et al. (1985)) around early type galaxies. The X-ray surface brightness profile was found to closely follow the optical image (Trinchieri et al. (1986)) although closer inspection revealed that the X-ray spectrum consists of both a hard and soft component. The hard X-ray component of the luminosity is found to be proportional to the blue band luminosity of the galaxy (Trinchieri et al. (1986)), suggesting that the origin of this component is due to low-mass X-ray binary stars. The soft component of the X-ray spectrum can be explained in terms of thermal Bremsstrahlung emission from hot gas (Fabbiano et al. (1994)) and as such can be used as a probe of the temperature structure
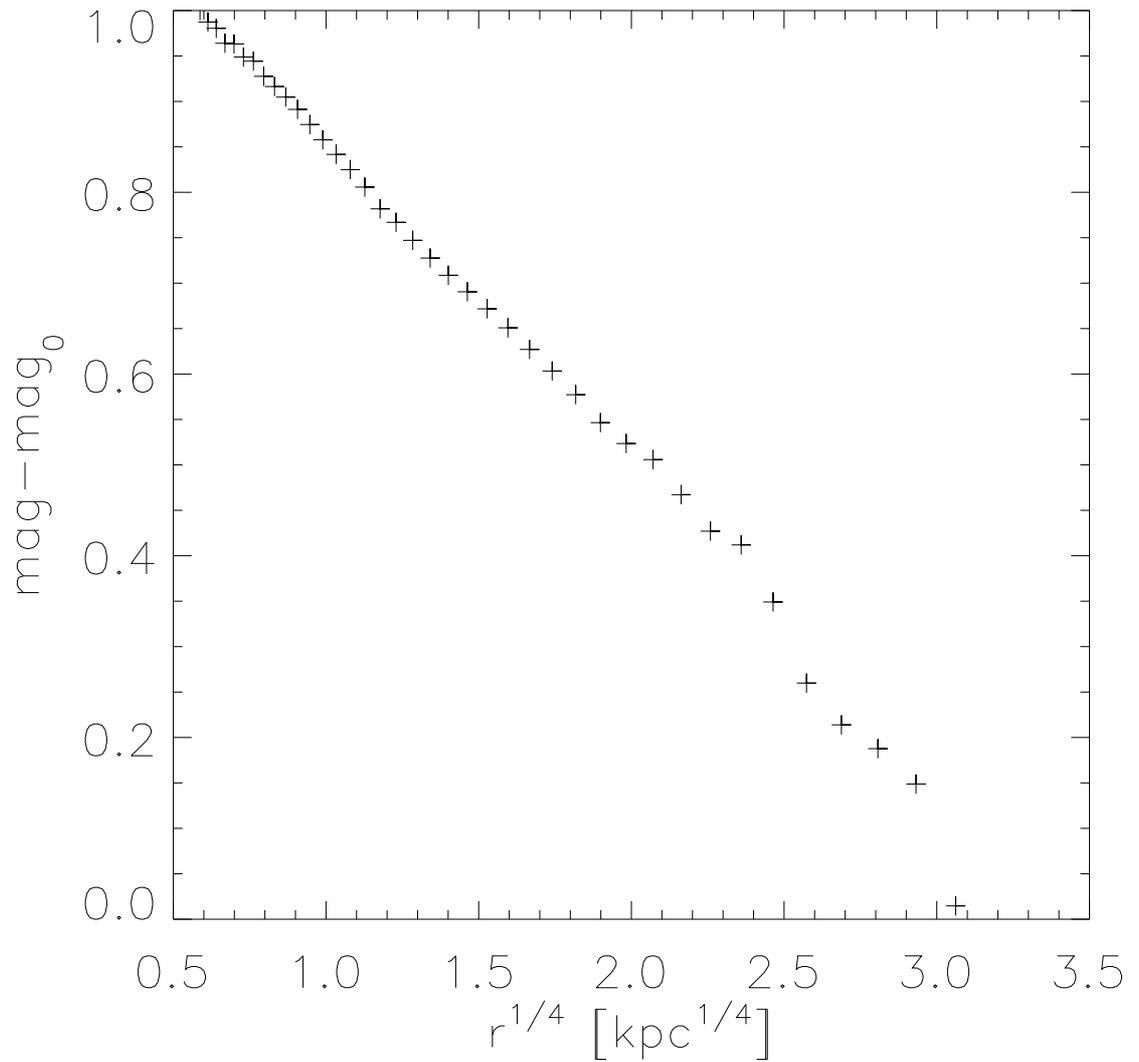
Figure 5.8: Projected surface brightness profile of the merger remnant. Magnitudes were calculated from stellar masses by assuming that the flux from any given particle is proportional to its mass, then calculating the magnitude from $m = -2.5 \log(flux)$.
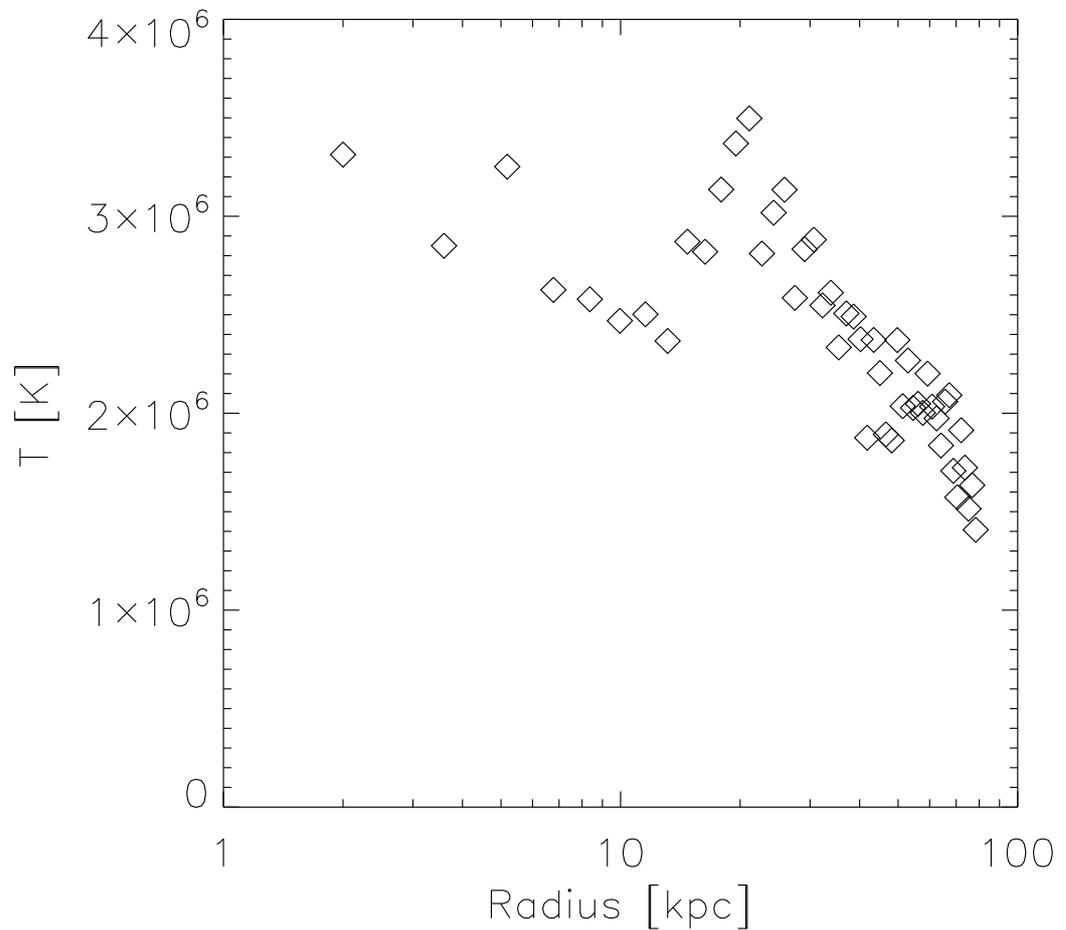
Figure 5.9: Three dimensional temperature profile of the merger remnant, we find a negative temperature gradient in the halo. This is in agreement of recent X-ray observations of local early type galaxies, which have found that in haloes with masses less than $10^{13}M_\odot$ there is a negative temperature gradient

of the hot phase of the ISM

Figure 5.9 shows the three dimensional temperature profile of the resulting elliptical galaxy. We find a shallow negative gradient to the temperature profile. This result is in agreement with the observations of Humphrey et al. (2006) (see also Randall et al. (2006); Khosroshahi et al. (2004)), who found that galaxies with halo masses $< 10^{13}M_\odot$ tended to have negative temperature profiles

In this chapter we have examined some of the properties of interacting galaxies, we find that we create realistic tidal features and that the resulting merger remnant has many properties in common both with other simulations and the observed properties of early type galaxies in the local universe. These features include density and brightness profiles, the temperature gradient in the galaxy and the appearance of strong bursts of star formation in tidal structures.

5.6   The ISM in a Cosmological Setting

Galaxies do not evolve in isolation and the effects of the surrounding intergalactic medium and mergers with other galaxies play important roles in shaping the properties of the galaxies we observe today. It is therefore important to be able to understand how galaxies form in a fully self consistent cosmological context. As a final test of the code we therefore attempt to simulate a MW-like galaxy picked from a cosmological volume.

In order to facilitate a comparison of our results with those obtained using different codes we use the initial conditions first developed by Okamoto et al. (2005). These initial conditions represent the formation of a single high resolution halo in a volume of 35.325 Mpc/h. The cosmology used is $\Omega_0 = 0.3$, $\Omega_\Lambda = 0.7$, $\sigma_8 = 0.9$, $h_{100} = 0.7$. The gravitational softening for the high resolution parts of this simulation is $\epsilon = 1.4$ kpc. The numerical parameters governing the behaviour of the sticky particle model are exactly the same as those used in the earlier simulations of both isolated and interacting galaxies.

5.6.1   Results

Figure 5.10 shows the projected density of each phase of the ISM at redshift zero. Both the molecular and atomic phases of the ISM are confined to a thin (~ 1 kpc) disk, whereas the stellar disk has a significantly larger scale height. The radial density profile of the ambient and molecular ISM phases are shown in figure 5.11. It is clear that at the centre of the galaxy the ISM is primarily molecular, and at the outskirts it is almost entirely atomic, qualititatively the shapes of the two density profiles match well with those found in the local universe (e.g. Dame et al. (1993); Binney and Merrifield (1998)). This finding is consistent with the results found in chapter 4 for an isolated model halo, and provides confirmation that our approach towards modeling can provide insight into the properties of the molecular ISM in low redshift galaxies. The molecular fraction in the galaxy $(N(H_2)/(N(H_2) + N(HI)))$ as a function of radius also agrees well with that observed

in the local universe (for comparison see figure 4.10).

Figure 5.13 shows the radial density profile of the stellar component of the galaxy. This distribution is well fitted by a Vaucouleurs law, representing a bulge component

$$\Sigma(r) = \Sigma_{0,b} e^{[-(r/r_b)^{0.25} - 1]} , \tag{5.4}$$

and an exponential disk

$$\Sigma(r) = \Sigma_{0,d} e^{-(r/r_d)} . \tag{5.5}$$

We find that the values of the scale lengths, r_b and r_d, needed to describe the simulated galaxy are $r_d = 4$kpc, the bulge component has a scale length of $r_b = 0.8$kpc.

Finally the same halo was simulated using different star formation and feedback prescriptions, including the code from Okamoto et al. (2005) and the Gimic code[2], which has been developed to perform large scale simulations of galaxy formation. Comparing the star formation histories of the galaxies generated with each code (figure 5.14) we find that the total mass in stars is very similar between the sticky particle simulation and the run using the Gimic code, differing only by $\sim 10\%$ at redshift zero. The Okamoto et al. (2005) code forms more stars by a factor of two. However, we note that at high redshift the sticky particle code forms significantly more stars than the other codes. This is due to its crude treatment of metal production, more specifically the assumption that the metallicity is constant and equal to the solar value at all redshifts. This leads to radiative cooling rates for the gas that are orders of magnitude larger than those for zero metallicity gas and results in an efficient and early collapse of much material.

In this section we have demonstrated that the sticky particle star formation model does a good job of reproducing many of the observed properties of galaxies in the low redshift universe, including: The density profiles of all of the phases of matter, star formation rates over the entire lifetime of the galaxy and the molecular fraction of the galaxy as a function of radius. Possible future directions in which this work may be taken are described in chapter 6.

---

[2]We thank our colleagues J. Schaye, C. Dalla Veccia and R. Wiersma for allowing us the use of this code, and R. Crain for performing this simulation
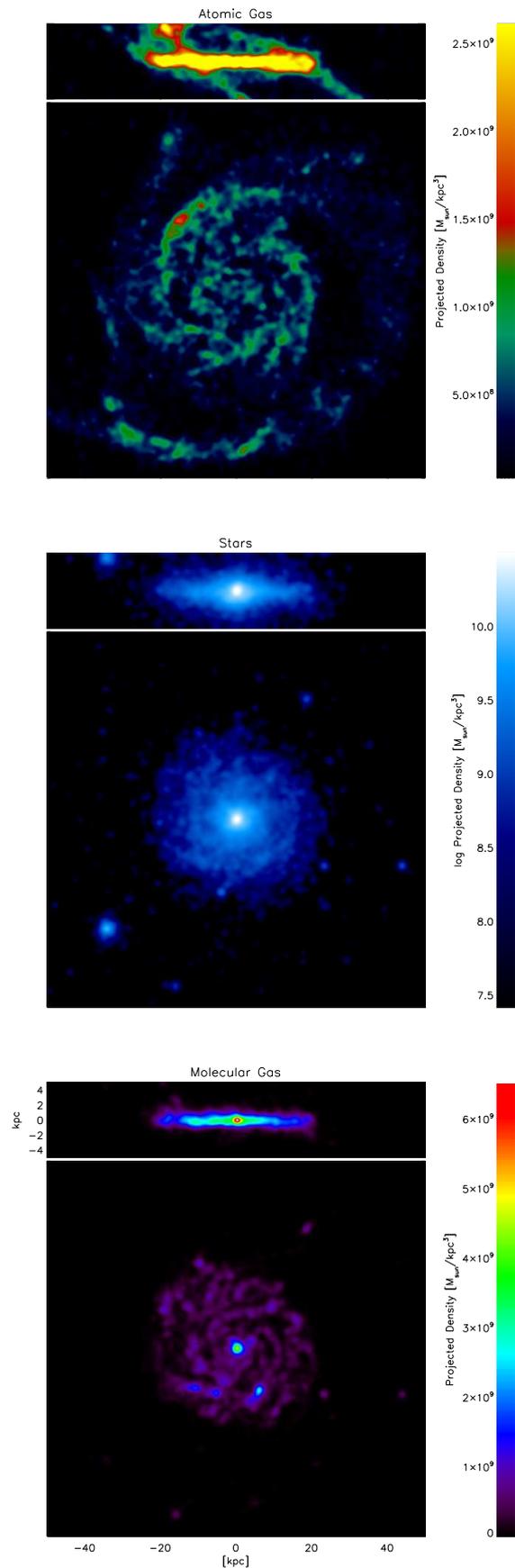
Figure 5.10: Projected density through the redshift zero galactic disk for each of the three baryonic components included in our simulations
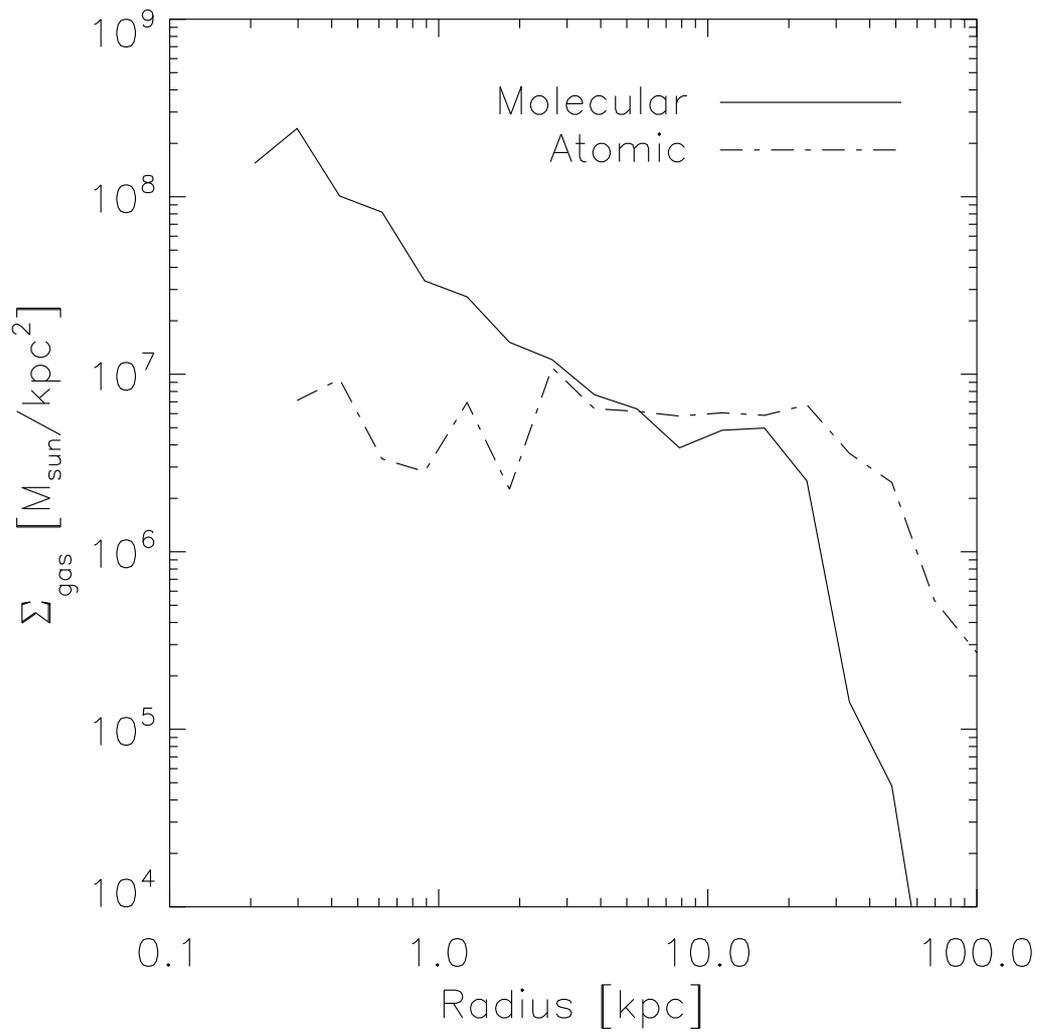
Figure 5.11: Radial density profiles for the hot atomic (SPH) and cold molecular (sticky particle) gas phases in the redshift zero galactic disk. It is clear that near the centre of the galaxy most of the gas is molecular, whereas on the outskirts the galaxy is primarily atomic
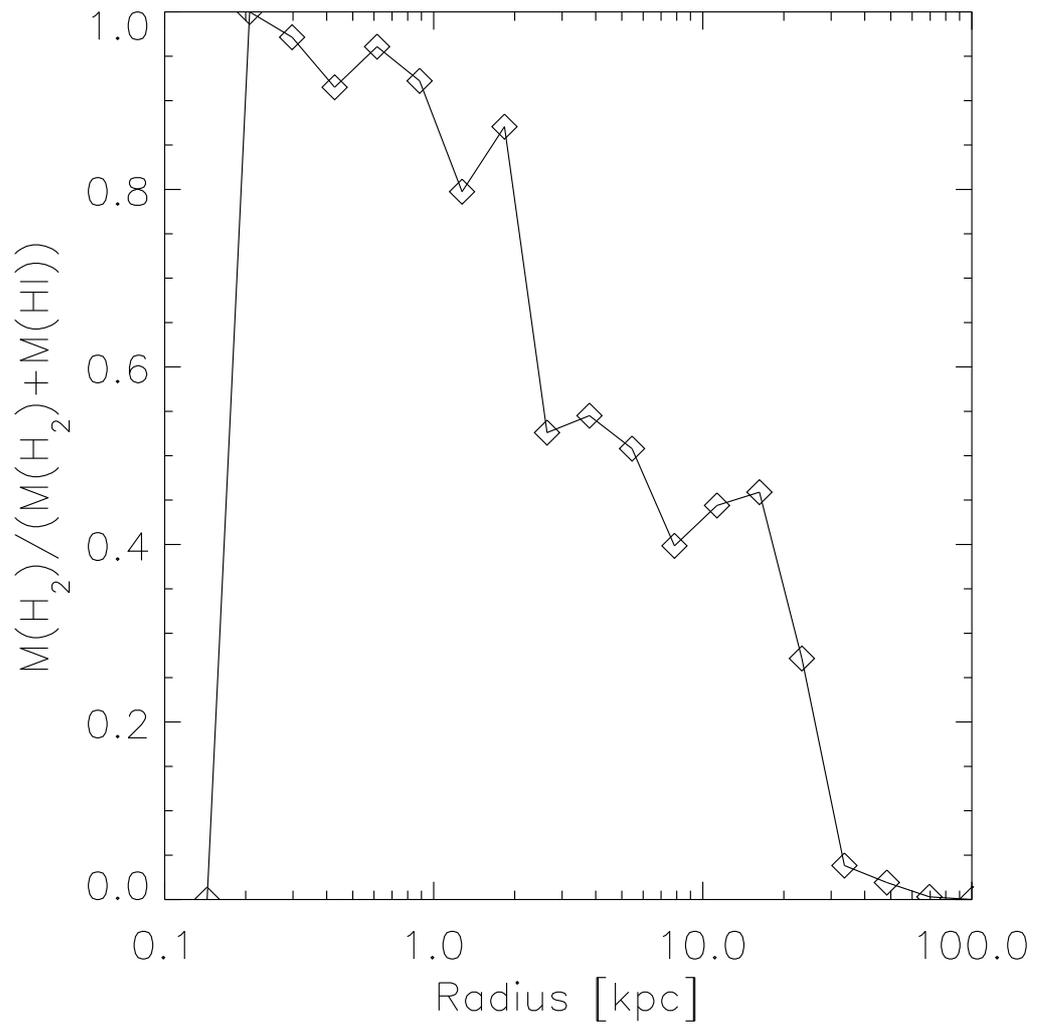
Figure 5.12: Proportion of molecular gas as a function of distance from the centre of the galaxy at redshift zero
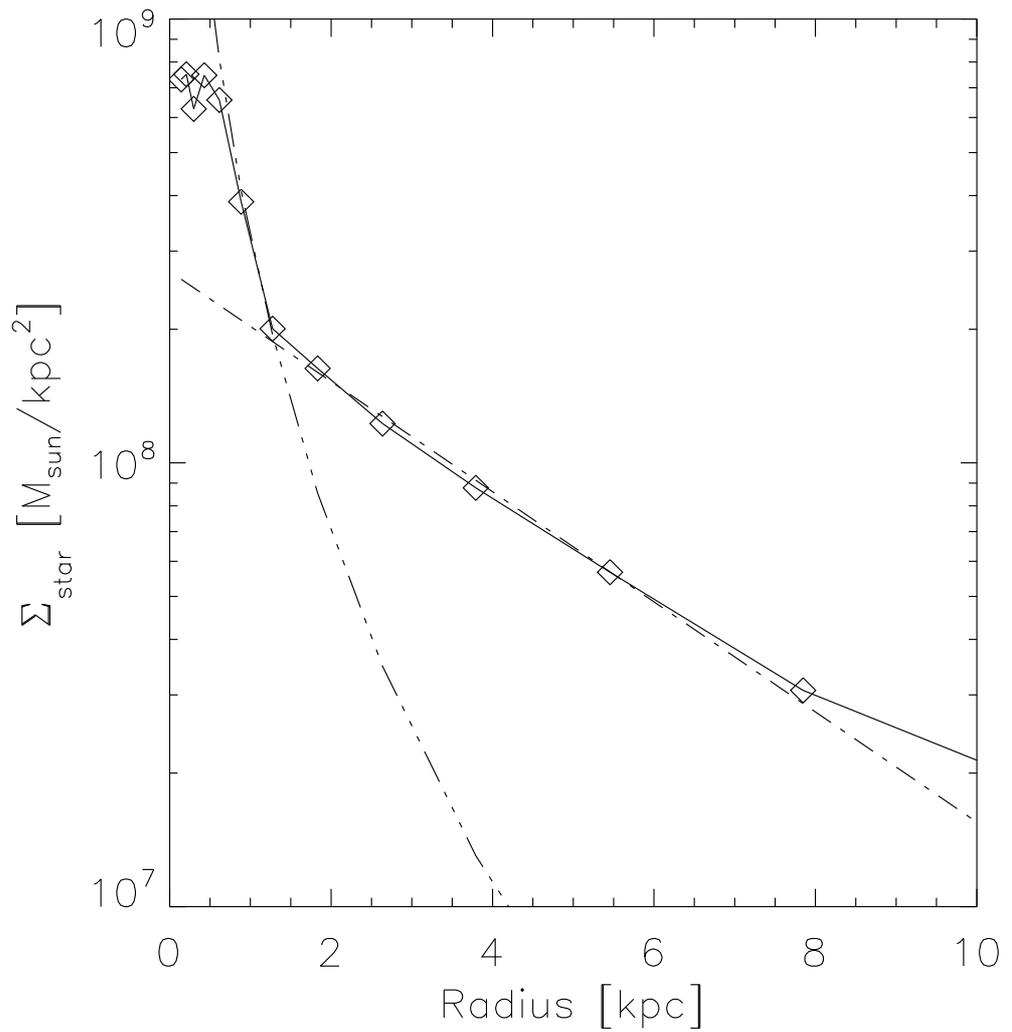
Figure 5.13: Stellar radial density profile of the redshift zero disk. The two dashed lines represent a best fit bulge and disk component for the galaxy.
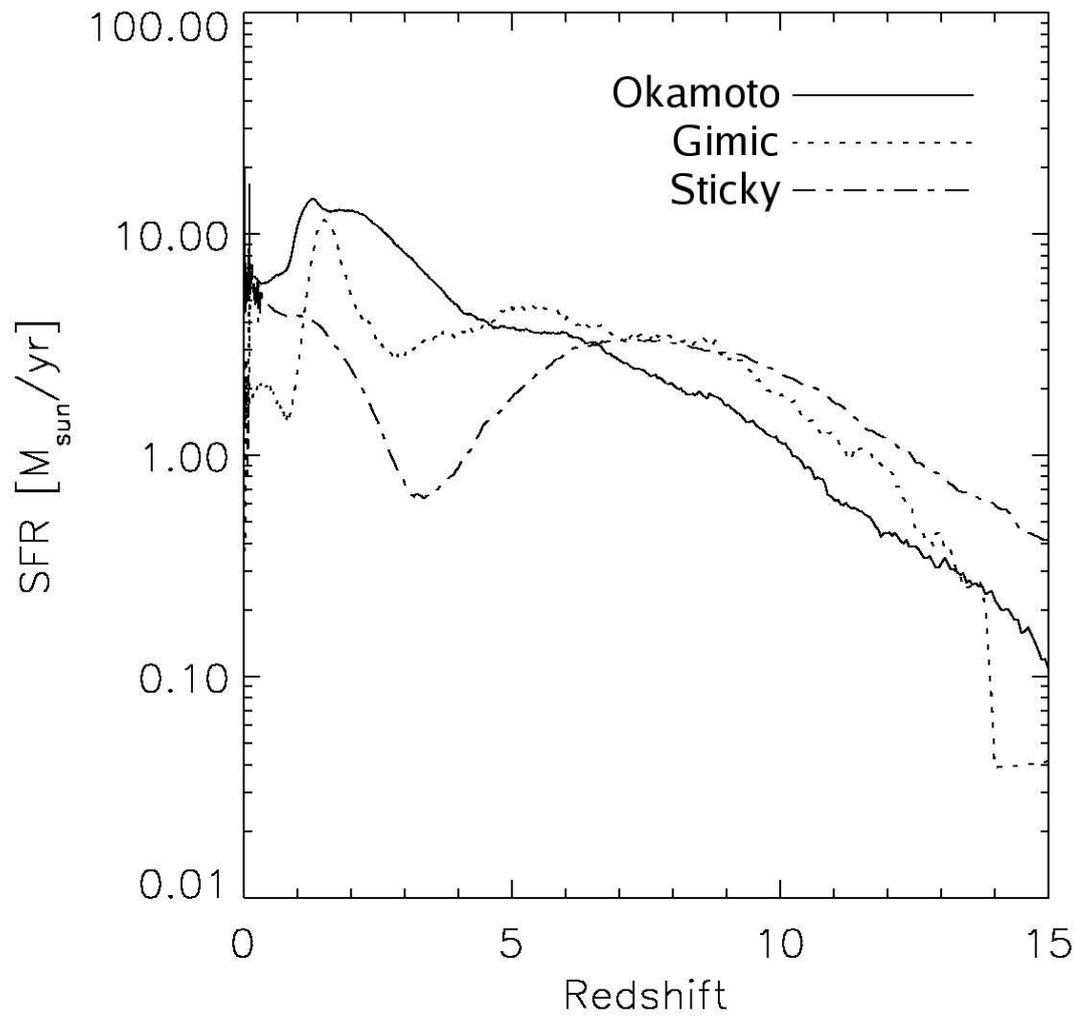
Figure 5.14: Comparison of star formation histories of the same galaxy run with three different codes. The three different codes are described in the text.